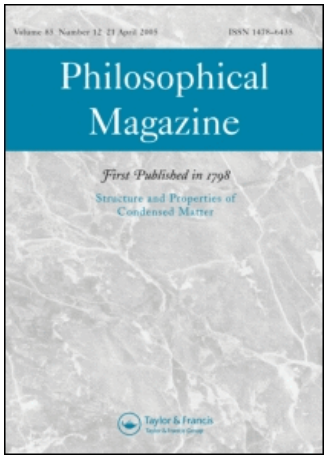

Philosophical Magazine
First published in 1798
Publication details, including instructions for authors and subscription information:
http://www.informaworld.com/smpp/title~content=t713695589

Nitrogen doping and multiplicity of stacking faults in SiC

P. Pirouz [a]; M. Zhang [a]; H. McD. Hobgood [b]; M. Lancin [c]; J. Douin [d]; B. Pichaud [c]
[a] Department of Materials Science and Engineering, Case Western Reserve University, Cleveland, OH 44106, USA
[b] Cree Inc., Durham, NC 27703, USA
[c] Laboratoire TECSEN, Université Paul Cézanne, 13397 Marseille Cedex 20, France
[d] CEMES-CNRS, 31055 Toulouse Cedex 04, France

Online Publication Date: 11 October 2006
To cite this Article: Pirouz, P., Zhang, M., Hobgood, H. McD., Lancin, M., Douin, J. and Pichaud, B. (2006) 'Nitrogen doping and multiplicity of stacking faults in SiC', Philosophical Magazine, 86:29, 4685 - 4697
To link to this article: DOI: 10.1080/14786430600724470
URL: http://dx.doi.org/10.1080/14786430600724470

Philosophical Magazine,
Vol. 86, Nos. 29–31, 11 Oct.–1 Nov. 2006, 4685–4697

Taylor & Francis
Taylor & Francis Group

Nitrogen doping and multiplicity of stacking faults in SiC

P. PIROUZ*†, M. ZHANG†, H. McD. HOBGOOD‡, M. LANCIN§, J. DOUIN¶ and B. PICHAUD§

†Department of Materials Science and Engineering, Case Western Reserve University, Cleveland, OH 44106, USA
‡Cree Inc., Durham, NC 27703, USA
§Laboratoire TECSEN, Université Paul Cézanne, Aix–Marseille III, 13397 Marseille Cedex 20, France
¶CEMES-CNRS, 31055 Toulouse Cedex 04, France

(*Received 30 November 2005; in final form 3 March 2006*)

This paper reports on the strong enhancement of stacking fault (SF) formation in 4H–SiC by heavy nitrogen doping. The paper consists of two separate observations. The first part reports on localized but severe deformation bands observed in certain regions of 4H–SiC wafers that had undergone high temperature processing during device fabrication. Using a combination of dynamic secondary ion mass spectroscopy (SIMS) and conventional, weak-beam (WB) and high-resolution (HR) transmission electron microscopy (TEM), the affected regions of the wafers were found to have a much higher concentration of nitrogen and to contain a high density of stacking faults. In contrast, in the non-affected regions of the wafers, the nitrogen concentration was lower and no lattice defects could be observed by TEM, indicating that the severely deformed morphology of the affected regions was due to the high stacking fault content. Moreover, the stacking faults in the affected regions were found to be invariably double and not single-layered, formed by the glide of two leading partial dislocations on adjacent (0001) planes. The second part of the paper reports on the occurrence of stacking faults during deformation tests on heavily nitrogen-doped 4H–SiC. Combining optical microscopy, HR and weak-beam (WB) TEM, the generated faults were found to be double-layered as well. It is interesting that in neither type of experiment, trailing partials were observed: it appears that the SFs were not in the form of ribbons bound by leading and trailing partials but rather in the form of faulted loops on two adjacent planes, each loop bound by a leading Shockley partial of the same Burgers vector. The results of the two observations are explained by the stabilization of double-layer stacking faults (DSFs) when the Fermi level of the faulted crystal is pushed up by nitrogen doping to above the stacking fault energy level.

1. Introduction

Once it was recognized that dislocations in crystals can be imaged in an electron microscope by their strain field [1, 2], and the development of column approximation allowed calculation of dislocation image contrast [3–5], procedures for defect

*Corresponding author. Email: pxp7@cwru.edu

Philosophical Magazine
ISSN 1478–6435 print/ISSN 1478–6443 online © 2006 Taylor & Francis
http://www.tandf.co.uk/journals
DOI: 10.1080/14786430600724470

characterization were developed and rapidly applied to real materials. Some of the first applications of TEM to characterize dislocations were in semiconducting materials, and specifically to silicon [6–8]. Since then, TEM has been instrumental in characterizing dislocations in a variety of semiconductors, determining their Burgers vectors, slip planes and whether they are dissociated into partial pairs or not. The use of strain contrast technique, particularly WBTEM [9], also made possible the measurement of stacking fault energy (SFE). In this paper, we report on two recent phenomena, both dealing with the occurrence of stacking faults (SF), which happen to be double-layer (DSF) in every case, in the wide bandgap semiconductor, 4H–SiC. In both these studies, TEM played a major role in characterizing the defects in the material – predominantly planar in nature – and helped elucidate the reasons behind the occurrence of an abnormally high DSF density.

2. Experimental and results

2.1. *Stacking fault formation during high-temperature processing of 4H–SiC wafers*

In the first part of this section, we discuss spontaneous occurrence of stacking faults during high temperature device processing of 4H–SiC wafers heavily doped with nitrogen [10]. The samples examined were commercial 2″ 4H–SiC wafers with a thickness of ~500 μm on which 4–5 μm thick epilayers were homoepitaxially grown (see the schematic of a wafer in figure 1). Such wafers are often used for the fabrication of 4H–SiC Schottky diodes. In the processing stage of some of these wafers, it was visually noticed that severe localized deformation bands had formed in certain regions of some of the wafers (figure 2). The dashed line QQ′ in the schematic drawing of figure 1 delineates the approximate boundary separating the affected (region B) and unaffected (region A) parts of the wafer. As shown in this schematic, small samples for TEM study and SIMS analysis were cut from the two regions of the processed wafer. Moreover, while Schottky diodes fabricated from

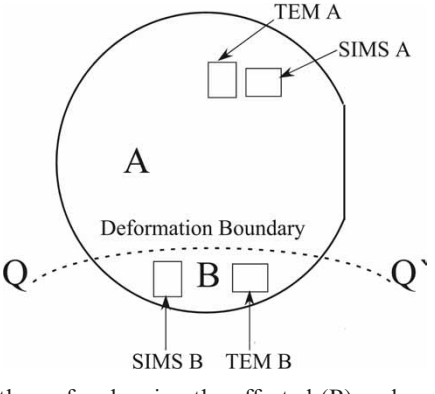

Figure 1. Schematic of the wafer showing the affected (B) and unaffected (A) regions from which TEM and SIMS specimens were taken.

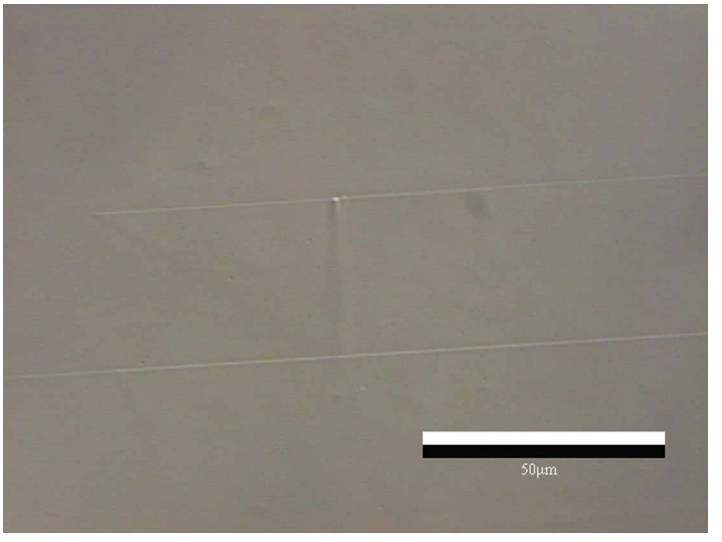

Figure 2. Optical micrograph of the affected region of a processed wafer. A high density of line features, such as two near-horizontal lines in the figure, appear in this region.

the non-affected regions of the wafers exhibited normal resistivity characteristics, those made from the affected regions exhibited a significantly higher resistivity and an increased forward bias. Since the crystals were grown in a nitrogen environment, the processed wafers were first analyzed by dynamic secondary ion mass spectrometry (SIMS). SIMS analysis showed a gradient in nitrogen doping with the affected regions having a higher nitrogen content than the other parts of the wafer. Figure 3a is a SIMS profile showing nitrogen concentration as a function of depth from the wafer surface taken from region A, where the top $\sim$5 μm corresponds to the epilayer. As seen in this figure, there is a sharp transition in nitrogen doping at the interface where the donor concentration increases by nearly three orders of magnitude from $\sim 10^{16}\,\mathrm{cm}^{-3}$ in the epilayer to $\sim 1.0 \times 10^{19}\,\mathrm{cm}^{-3}$ in the substrate. The signal from the carbon matrix is shown for reference. The change in the concentration of boron and carbon between the epilayer and substrate was insignificant. The SIMs profile from region B, shown in figure 3b, indicates a higher nitrogen concentration of $\sim 2.7 \times 10^{19}\,\mathrm{cm}^{-3}$ in the substrate, nearly three times larger than the corresponding one in region A. This was the first indication that the substrate in the affected regions of the wafer had a significantly higher nitrogen concentration than that in the non-affected regions.

To investigate and characterize the defects giving rise to the deformed morphology of region B, the affected and non-affected regions of the wafer were examined and compared by TEM. Owing to the homoepitaxial nature of growth, it was difficult to distinguish the epilayer/substrate interface in either region. The distinct difference between the two regions turned out to be the presence of a high density of SFs in the highly n-doped, affected region as compared to the lower-doped non-affected region. In fact the defect density in the latter part is low enough that practically nothing shows up in TEM observations. Figure 4 shows a typical low

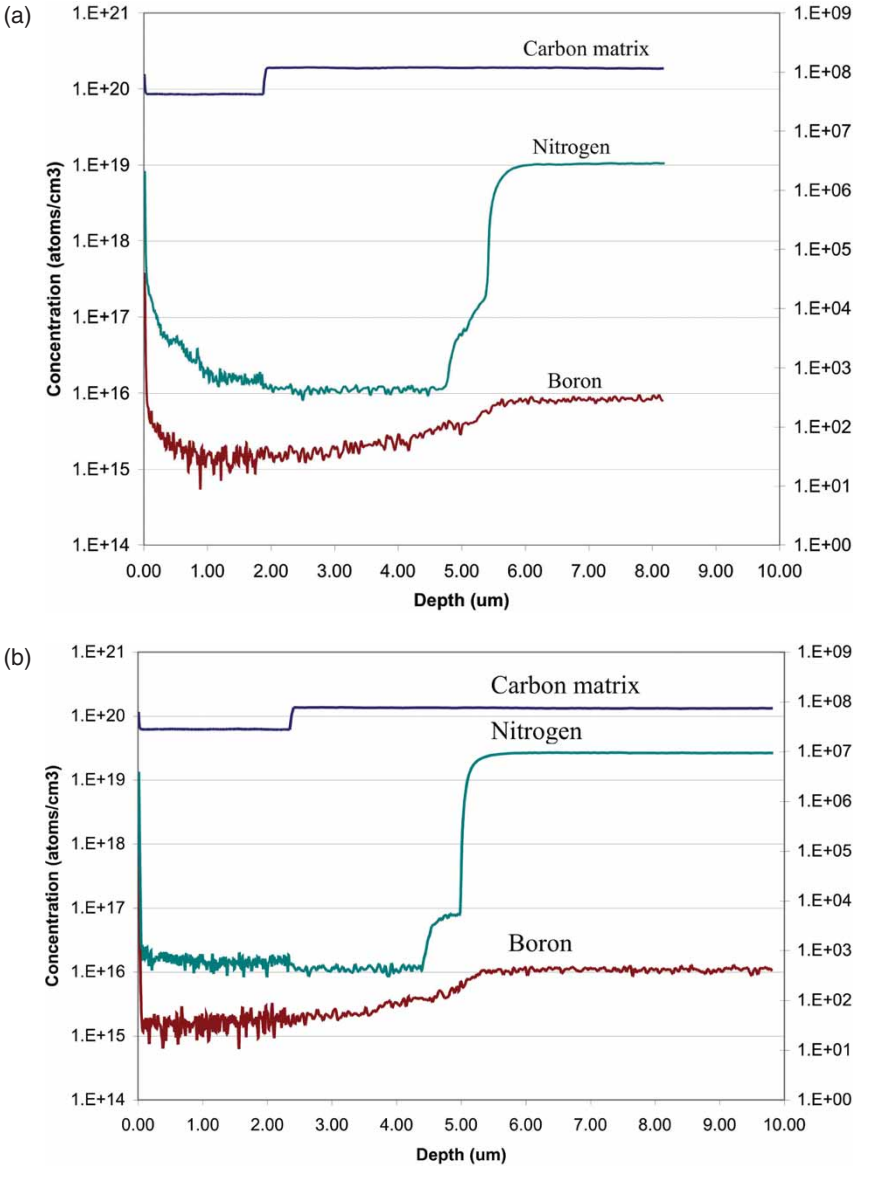

Figure 3. SIMS spectra from near the epilayer/substrate interface showing the nitrogen profile. In the epilayer, extending from the surface to a depth of approximately 5 μm, the nitrogen concentration is low ($\approx 10^{16}\,cm^{-3}$). The substrate, starting at a depth of ~5 μm, has a higher nitrogen concentration of $\sim 1.1 \times 10^{19}\,cm^{-3}$ in region A (a) and $\sim 2.7 \times 10^{19}\,cm^{-3}$ in region B (b).

magnification cross-sectional TEM micrograph of the epilayer/substrate interface in a specimen prepared from region B (severely deformed region of the processed wafer). A high density of straight dark lines, corresponding to the projection of stacking faults on different (0001) planes, can be observed randomly distributed in

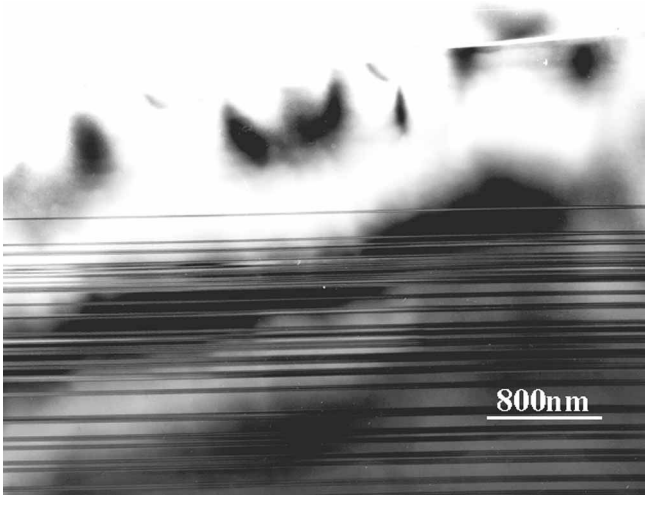

Figure 4. Low-magnification bright-field cross-sectional TEM micrograph of the interface between the substrate (lower defective part) and epilayer (upper defect-free part) in the affected part (region B) of the processed wafer. The straight, near-horizontal lines are intersection of (0001) stacking faults with the $(11\bar{2}0)$ foil surface.

the lower substrate part of the micrograph, separated from a clean, defect-free, region, in the upper epilayer portion. It is significant that hardly any defect could be observed in TEM specimens prepared from the unaffected A region of the processed wafer, indicating that a change of nitrogen concentration in the substrate from $\sim 1.0 \times 10^{19}$ to $\sim 2.7 \times 10^{19}\,\mathrm{cm}^{-3}$ (region B) has resulted in a dramatic increase in the stacking fault density.

The stacking faults in the affected region of the wafer were examined by HRTEM and, in the cases imaged, were found to be invariably double-layered. A typical high-resolution TEM micrograph of a few of the dark lines in figure 4 is shown in figure 5b. For comparison purposes, an HRTEM micrograph of a perfect 4H–SiC crystal is shown in figure 5a. Under the defocus conditions used in these HRTEM micrographs, each white spot corresponds to the projection of a normal or twinned variant of a Si–C tetrahedron that assemble to make a SiC structure (see, for example [11]). In perfect 4H–SiC, the stacking sequence is $T_1T_2T_1'T_2'$ where T and T' represent normal and twinned variants of Si–C tetrahedra, respectively; in the Zhdanov notation [12] this is represented as 22 (two normal and two twinned variants). The stacking sequence in a single-layer stacking fault (SSF) is 31 (three normal and one twinned variant) and in a double-layer stacking fault (DSF) is 62 (six normal and two twinned variants). In fact, a six-layer band of cubic polytype in HRTEM micrographs of 4H–SiC is the signature of a double-layer stacking fault, just as a three-layer cubic band is the signature of a single-layer stacking fault.

In figure 5b, some of the six layer bands with a cubic stacking sequence can be clearly seen. As previously mentioned, all the stacking faults in the affected region of the wafer turned out to be DSFs and no single-layer stacking faults were ever observed. It is thus reasonable to assume that the higher nitrogen content in the

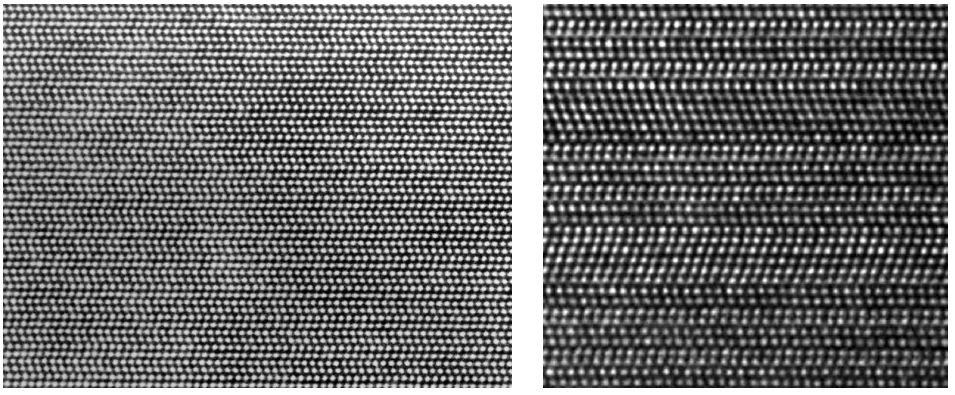

Figure 5. HRTEM micrograph of (a) a perfect region of 4H–SiC crystal and (b) double-layer stacking faults in the damaged region. In both figures, the incident beam, normal to the plane of the micrographs, is along the [11$\bar{2}$0] direction and the *c*-axis is vertical. The spacing between the spots in the vertical [0001] direction, equal to spacing between basal *c* planes, is ~0.25 nm.

affected regions of 4H–SiC corresponded with the high density of DSFs. A number of questions arise, the most important of which is probably the driving force for the glide of the leading Shockley partials that are responsible for the stacking faults, and why double- and not single-layer stacking faults are forming. Before we address these questions in section 3, the second set of observations will be summarized below.

2.2. *Stacking fault formation during bending experiments on nitrogen-doped 4H–SiC*

The second part of this review reports on some bending experiments in highly n-doped 4H–SiC [13, 14]. Dislocation sources were introduced by a scratch on the (11$\bar{2}$0) surface of $20 \times 5 \times 0.2\,\mathrm{mm}^3$ parallelepiped samples which had a nitrogen concentration of $5 \times 10^{18}\,\mathrm{cm}^{-3}$. Two series of samples I and II underwent different treatments: series I samples were only scratched and annealed, while series II samples were scratched, bent plastically at room temperature and subsequently annealed at 550°C for 30 min. After treatment, each sample was initially etched and examined by an optical microscope. In addition, slices were cut parallel to (0001) for WBTEM, and parallel to (11$\bar{2}$0) for HRTEM. The (11$\bar{2}$0) slices were polished and ion-beam thinned to electron transparency, while the (0001) slices were selectively thinned by the focused ion-beam (FIB) technique in the regions where the faults intersected the sample surface. Optical and electron microscopy examination of the deformed samples showed that a high density of stacking faults had been generated in both series of samples. The optical micrographs in figures 6a and b show chemically-etched samples from the two series. The inclined dark lines at 45° with respect to the scratch line in both figures arise from the intersection of the stacking faults on parallel (0001) planes with the (11$\bar{2}$0) top surface of the sample. The stacking faults

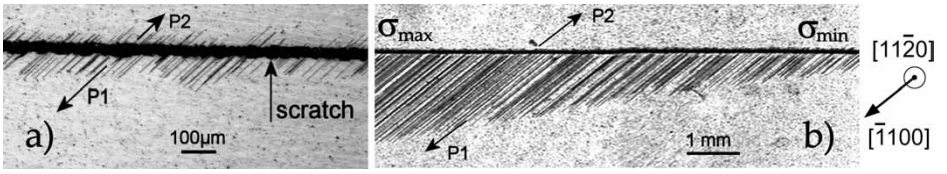

Figure 6. Optical micrograph of the (11$\bar{2}$0) surface chemically etched with molten KOH for 10 min at 500°C: (a) a series I sample annealed at 700°C for 30 min without bending; (b) a series II sample cantilever bent at room temperature and annealed at 550°C for 30 min.

were presumably nucleated as faulted partial half-loops on parallel (0001) planes from the scratch, with the half-loops expanding on their glide planes along $P_1 = [\bar{1}100]$ and $P_2 = [1\bar{1}00]$ directions. The systematic increase of the line length from right to left along the direction P_1 in figure 6b is due to the non-uniform compressive stress σ, which increases along the length of the sample from zero on the right hand side to a maximum value $\sigma_{max} = 170$ MPa on the left hand side.

Interestingly, HRTEM examination of (11$\bar{2}$0) thin foils indicated that all the examined stacking faults in both series were double-layered (DSFs) with six layers in a cubic stacking sequence; similar to that shown in figure 5b. This indicates that two faulted half-loops, bound by two Shockley partials, were expanding on two adjacent (0001) planes, giving rise to a DSF. In the central part of figure 7, a [11$\bar{2}$0] projection of charge density is shown with small and large spots indicating carbon and silicon atoms, respectively. To the right of this is an HRTEM micrograph of the bent sample showing the sense of shear and expansion of the fault along P_1 under the applied stress; a simulated image is superimposed on the left hand side of the experimental micrograph.

In addition to HRTEM, weak-beam microscopy on the (0001) specimens near the intersection of the faulted loops with the sample surface indicated that the bounding partials always had the same Burgers vector. An example of a typical WB micrograph of the two bounding partials on adjacent (0001) planes is displayed in figure 8; in figure 8a, stacking faults are out of contrast and only the two partial dislocations can be observed, whilst in figure 8b, a reflection is used that displays overlapping stacking faults. Note in figure 8a how the line directions of the two partials remain straight and parallel to the [$\bar{1}2\bar{1}0$] Peierls valley. Combining WBTEM and HRTEM, together with image contrast simulations [15] and core reconstruction [16] enabled us to determine both the Burgers vector **b** and core nature of the bounding partials in series I and II samples. As an example, the core composition of the two 30° partial pairs aligned along the [$\bar{1}2\bar{1}0$] Peierls valleys, and dragging the DSF in figures 7 and 8, is displayed as a charge density projection in figure 9. The core reconstruction was realized in the ($\bar{1}2\bar{1}0$) plane perpendicular to each dislocation line to obtain the structural unit (hatched cycles), characteristic of 30° partials belonging to the glide set. Three faulted cycles linked by a column of silicon atoms – as shown in figure 9 – is characteristic of a partial with a silicon core. By drawing Burgers circuits around the [$\bar{1}2\bar{1}0$] line direction (perpendicular to the page) in figure 9, using the SF/RH convention together with the results from WBTEM, the Burgers vectors of the partials were determined. In every case

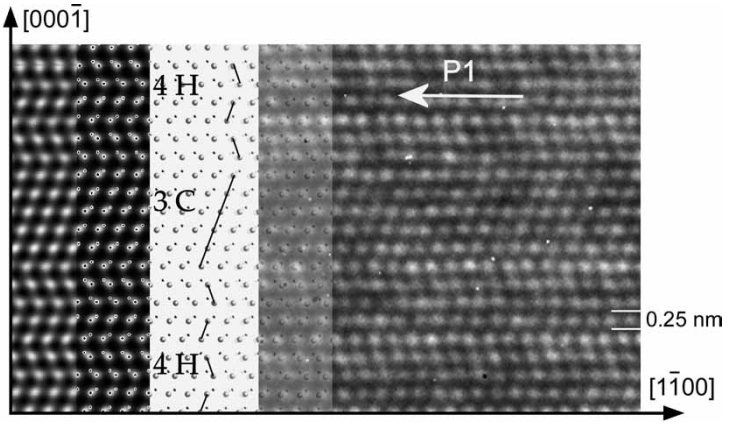

Figure 7. Left and centre parts show [11$\bar{2}$0] projection of charge density, with small and large spots indicating carbon and silicon atoms, respectively. The experimental HRTEM micrograph on the right hand side shows the sense of shear and expansion of the fault along P_1 under the applied stress; a simulated image is superimposed on the left hand side of the experimental micrograph. Note that the experimental image was taken under a defocus condition whereby atom columns appear as white.

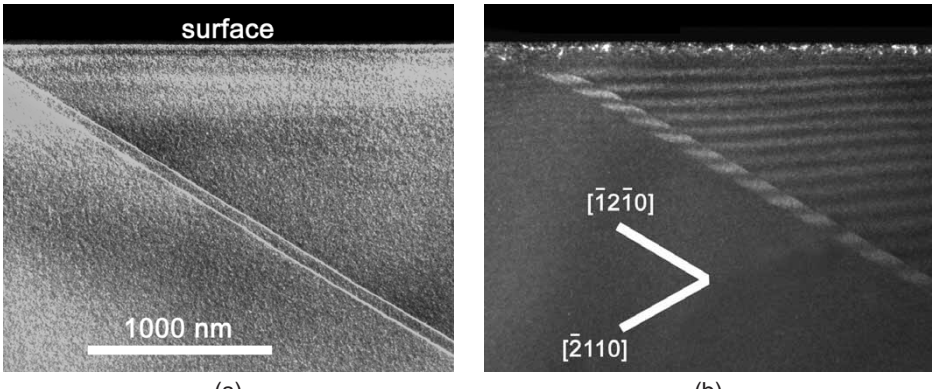

Figure 8. Weak-beam TEM micrographs of a DSF, similar to that shown in figure 7, with stacking faults on two adjacent planes (a) out of contrast; (b) in contrast. When the stacking faults are out of contrast, as in (a), only the two bounding Shockley partials can be seen.

examined, the Burgers vector of the two partials on adjacent (0001) planes turned out to be the same and, assuming the partial dislocations belong to the glide set, the core nature of the segments were Si(g). Among the 118 DSFs examined, not one segment was found to be C(g) implying a much lower mobility for these segments as compared to the Si(g) segments. This also explains the asymmetry of the etch-pit pattern in figure 6b and is consistent with previous results on plastic deformation of 4H–SiC [17]. In both series, the DSFs remaining close to the scratch are dragged by

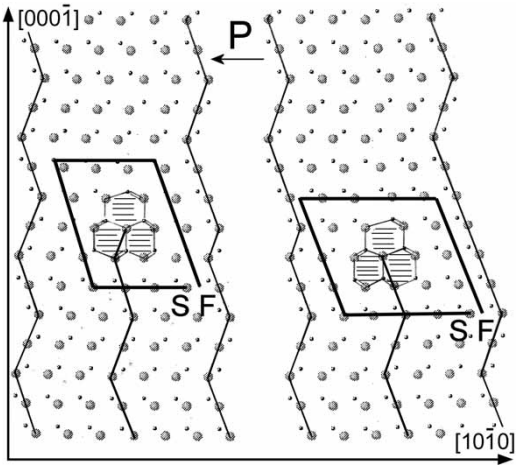

Figure 9. Core configuration of the two 30° partial dislocations displayed in figure 8 is shown as projections of charge density. Note that the [1$\bar{2}$10] projection of the atomic structure in this figure is a (1$\bar{1}$00) mirror of the [11$\bar{2}$0] projection in figure 7. In the drawing, P indicates the projection in the ($\bar{1}$2$\bar{1}$0) plane of the propagation direction of the partial dislocation. The partial core (hatched) consisting of three faulted cycles linked by a column of silicon atoms is characteristic of 30° Si(g).

Si(g) partial dislocations mostly exhibiting a 90° character, whilst the more extended DSFs (microns long) under the bending stress were always driven by 30° partial dislocations. It appears that initially, during scratching, faulted half-loops nucleate on two adjacent (0001) planes at different locations on the scratch [13]. During plastic bending, the half-loops expand asymmetrically with the most mobile segments of the bounding partials, i.e. the 90° Si(g), rapidly moving out thus leaving 30° segments behind [17]. The main question about the results of these experiments is the double-layer nature of the stacking faults. We shall discuss this below in terms of the quantum well action of single-layer (SSF), as well as double-layer stacking faults (DSF) [18, 19].

3. Discussion

The results presented in section 2.1 indicate that a high density of double-layered stacking faults are generated in the highly nitrogen-doped regions of the 4H–SiC wafer during high temperature processing of Schottky barriers and the defects give rise to an increased resistivity of the material. A somewhat similar phenomenon has been recently noted in PiN diodes fabricated from 4H–SiC. In this case, the operation of the diode, under forward biasing, results in its rapid degradation by the generation of a high density of stacking faults [20, 21]. However, in contrast to the present problem, where processed 4H–SiC wafers were used for the fabrication of Schottky diodes, the stacking faults in degraded PiN diodes are single- and not

double-layered [22]. In addition, it appears that in a bipolar device, such as a PiN diode, the high density of electron-hole pairs that are generated during device operation (forward biasing), recombine non-radiatively and the resulting recombination energy contributes to the glide of partial dislocations by effectively reducing the activation enthalpy for glide [23–25]. This is a well-known mechanism in semiconductors, called recombination-enhanced dislocation glide (REDG), and has been discussed extensively, e.g. in [26]. On the other hand, during the operation of a unipolar device, such as a Schottky diode, only one type of charge carrier is generated in excess and the recombination rate is not above the equilibrium value, i.e. REDG does not take place, and dislocation glide is not enhanced by the operation of the device.

Let us now consider the driving force for the glide of dislocations in a crystal. We assume that dislocations in semiconductors move on their slip planes by the Peierls mechanism, i.e. though the formation of kink pairs and sideways propagation of the kinks in opposite directions [27]. To have a bias in the formation and propagation of kinks and achieve a net motion of the dislocation line, a shear stress is generally needed that facilitates kink pair formation and propagation in one direction and slows it down in the other. If τ is the shear stress in the glide plane resolved in the direction of the dislocation Burgers vector **b**, then τb is the force per unit length of the dislocation line driving it in a direction normal to its line direction [27]. This applies to both perfect as well as partial dislocations. Clearly, there is no shear stress in the affected regions of the processed wafer, save for the small shear component that may be present because of the biaxial mismatch stress due to the difference in doping concentrations in the epilayer/substrate system. However, with a concentration difference of $\sim 10^3\,\mathrm{cm}^{-3}$ between the epilayer and the substrate, the biaxial stress and its shear component are too small to result in dislocation glide at temperatures as low as 500°C.

Besides shear stress, the only other driving force that could act to move a leading Shockley dislocation is a recently proposed electronic mechanism [18]. This is based on *ab initio* calculations by Miao *et al*. [18] as well as earlier calculations by Iwata *et al*. [28] on perfect and faulted 4H–SiC crystals that indicated, surprisingly, the production of an energy level (actually a narrow band) in the bandgap of the material by a (single-layer) stacking fault! This defect band is split off, and extends down to about 0.2 eV below the bottom of the conduction band of 4H–SiC. Based on this outcome, Miao *et al*. [18] proposed that a faulted n-type SiC crystal, with a Fermi energy above the defect level, is more stable than a perfect, unfaulted crystal. The reason for this is best understood if one thinks of a stacking fault as a two-dimensional quantum well with a depth equal to the 4H/3C conduction band offset ($\approx$0.7 eV) that can accommodate electrons from the conduction band of 4H–SiC, and effectively lower the free energy of the faulted crystal [19]. Specifically, if the difference between the Fermi level and the SF level is larger than the energy required to create an SF of energy γA (where A is the stacking fault area and γ is the SFE), then there is a driving force for the creation of the stacking fault. In other words, in this case, the faulted crystal will have a lower free energy than a perfect crystal and will, thus, be more thermodynamically stable than a perfect, unfaulted crystal. The calculations of Iwata [29] actually showed that a double-layer staking fault gives rise to an even deeper level (narrow band) in the bandgap of 4H–SiC, about 0.6 eV below

the bottom of the conduction band. In this sense, a 4H–SiC crystal containing double-layered stacking faults (DSFs) can be even more stable than one containing single-layered faults (SSFs), both having a lower free energy than a perfect crystal of 4H–SiC. The energy of intrinsic (single-layer) stacking fault in 4H–SiC has been experimentally measured to be $\gamma_{SSF} \approx 14.7\,mJ/m^2$ [30] and that of double-layered fault has been calculated to be $\gamma_{DSF} \approx 18.7\,mJ/m^2$ [31]. In the case when the Fermi energy is higher than the SF level, as more and more electrons from the conduction band start occupying the lower energy states of the quantum wells (stacking faults), a space charge builds up around the wells that makes accommodation of further electrons more difficult. Kuhr *et al.* [32] calculated the build-up of the space charge around the stacking faults and concluded that for a faulted crystal containing DSFs to be more stable than a perfect 4H–SiC crystal at the annealing temperatures under consideration (above 1000°C), the Fermi energy has to be appreciably higher than the DSF level, corresponding to a threshold doping concentration of $2 \times 10^{19}\,cm^{-3}$ (this needs to be even higher for the stability of a faulted crystal containing single-layer stacking faults whose energy level is closer to the bottom of the conduction band). The fact that a highly n-doped faulted crystal is more stable than a perfect crystal implies that there is a driving force for the formation of DSFs, proportional to the difference in the free energies of the faulted and unfaulted crystals. Also, since stacking faults form by the motion of the leading partial dislocations on the crystal slip plane, there is a driving force for the glide of leading Shockley partials. Of course, to kinetically drive (glide) a leading partial dislocation and produce a stacking fault, it must overcome the activation barrier for dislocation glide in 4H–SiC. The latter has been estimated to be about 2.5 eV for perfect dislocations [33], and about 1.3 eV for leading partial dislocations [34]. The large difference between these two activation energies may be because glide of perfect (dissociated) dislocations is controlled by the slow C(g) partial, whereas the partial dislocations whose velocity was measured by Idrissi *et al.* [34] were presumably the fast Si(g) partials. The energy to overcome this activation barrier is thermal in the case of processed wafers (provided during the high temperature processing step) and thermo-mechanical in the case of bending experiments (provided by the applied stress at intermediate temperatures).

Thus, as regards the first set of experiments, we conclude that the doping level in certain regions of the processed wafers under consideration exceeded the threshold doping ($>2 \times 10^{19}\,cm^{-3}$) for the onset of DSF generation during high temperature (>1000°C) processing. As a result, the local Fermi level in the highly doped regions was raised to a higher level than the DSF energy level, thus, making spontaneous formation of double-layer SFs energetically favorable. It is proposed that the presence of the SFs leads to reduced charge carrier mobility and, thus, reduced conductivity in the very highly doped regions. With regards to the second set of experiments, it is plausible that the threshold doping concentration for the formation of double stacking faults is much lower and is around $10^{18}\,cm^{-3}$ because the 4H–SiC crystal is experiencing a much lower temperature of around 500–600°C. Consequently, the Fermi energy is higher up in the bandgap, closer to the bottom of the conduction band and above the DSF energy level, thus, making the faulted 4H–SiC more stable.

4. Conclusion

It has been known for a long time that SiC crystals usually contain a high density of stacking faults and this has been attributed to the low stacking fault energy of this material ($<20\,mJ/m^2$). In this paper, we report on the application of TEM to study a recent phenomenon in 4H–SiC, i.e. the role of nitrogen in the formation of stacking faults. HRTEM has shown that the stacking faults in this case are double-layered (DSFs) and the DSFs may be forming by a new electronic mechanism. This mechanism arises because of two distinct characteristics of SiC; the first is polytypism in the material with the different polytypes having widely different bandgaps and the second is that single and double-layer stacking faults in hexagonal polytypes are structurally similar to cubic inclusions in a hexagonal matrix. Consequently, at the interface between the stacking faults (cubic inclusions) and the 4H–SiC matrix, there is a conduction band offset that can be as large as 0.7 eV. In this way, the stacking faults give rise to narrow energy bands in the bandgap of 4H–SiC and can act as quantum wells with energy levels appreciably lower than the bottom of the conduction band of the crystal. The consequence is that in a faulted 4H–SiC, the stacking faults (quantum wells) can accommodate electrons from the conduction band of the material and, thus, render its free energy lower. In this way, when the donor doping in the crystal is high enough to raise the Fermi level to above the DSF level, a faulted 4H–SiC crystal can actually be more stable than a perfect unfaulted crystal, implying that there will be a built-in driving force for the formation of stacking faults in SiC.

Acknowledgement

PP would like to thank the National Science Foundation for partial support of this work.

References

[1] P.B. Hirsch, R.W. Horne and M.J. Whelan, Phil. Mag. **1** 677 (1956).
[2] W. Bollmann, Phys. Rev. **103** 1588 (1956).
[3] P.B. Hirsch, A. Howie and M.J. Whelan, Phil. Trans. R. Soc. (Lond.) A **252** 499 (1960).
[4] A. Howie and M.J. Whelan, Proc. R. Soc. (Lond.) A **263** 217 (1961).
[5] A. Howie and M.J. Whelan, Proc. R. Soc. (Lond.) A **267** 206 (1962).
[6] H.J. Queisser, R.H. Finch and J. Washburn, J. Appl. Phys. **33** 1536 (1962).
[7] E. Aerts, P. Delavignette, R. Siems, *et al*., J. Appl. Phys. **33** 3078 (1962).
[8] G.R. Booker and R. Stickler, J. Appl. Phys. **33** 3281 (1962).
[9] D.J.H. Cockayne, I.L.F. Ray and M.J. Whelan, Phil. Mag. **20** 1265 (1969).
[10] M. Zhang, H.M. Hobgood, M. Treu, *et al*., Mater. Sci. Forum **457/460** 759 (2004).
[11] P. Pirouz and J.W. Yang, Ultramicroscopy **51** 189 (1993).
[12] G.S. Zhdanov, C.R. Acad. Sci. USSR **48** 39 (1945).
[13] M. Lancin, G. Regula, J. Douin, *et al*., in *Proceedings of International Conference on Silicon Carbide and Related Materials – 2005*, edited by R.P. Devaty, D.J. Larkin and S.E. Saddow (Trans Tech Publications, Zürich, 2006), in press.

[14] G. Regula, M. Lancin, H. Idrissi, *et al.*, Phil. Mag. Lett. **85** 259 (2005).
[15] P. Stadelmann, Ultramicroscopy **21** 131 (1987).
[16] M. Lancin, C. Ragaru and C. Godon, Phil. Mag. B **81** 1633 (2002).
[17] P. Pirouz, J.L. Demenet and M.H. Hong, Phil. Mag. A **81** 1207 (2001).
[18] M.S. Miao, S. Limpijumnong and W.R.L. Lambrecht, Appl. Phys. Lett. **79** 4360 (2001).
[19] U. Lindefelt and H. Iwata, in *Recent Major Advances in SiC*, edited by W.J. Choyke, H. Matsunami, and G. Pensl (Springer, Berlin, 2003), pp. 1–28.
[20] H. Lendenmann, F. Dahlquist, N. Johansson, *et al.*, Mater. Sci. Forum **353/356** 727 (2001).
[21] J.P. Bergman, H. Lendenmann, P.Å. Nilsson, *et al.*, Mater. Sci. Forum **353/356** 299 (2001).
[22] J.Q. Liu, M. Skowronski, C. Hallin, *et al.*, Appl. Phys. Lett. **80** 749 (2002).
[23] A. Galeckas, J. Linnros and P. Pirouz, Appl. Phys. Lett. **81** 883 (2002).
[24] P. Pirouz, M. Zhang, A. Galeckas, *et al.*, Mater. Res. Soc. Symp. Proc. **815** 91 (2004).
[25] A. Galeckas, J. Linnros and P. Pirouz, Phys. Rev. Lett. **96** 25502-1 (2006).
[26] K. Maeda and S. Takeuchi, in *Dislocation in Solids*, edited by F.R.N. Nabarro and M.S. Duesbery, Vol. 10, Chapter 54 (North-Holland, Amsterdam, 1996), pp. 443–504.
[27] J.P. Hirth and J. Lothe, *Theory of Dislocations* (Wiley, New York, 1982).
[28] H. Iwata, U. Lindefelt, S. Öberg, *et al.*, Mater. Sci. Forum **389/393** 533 (2001).
[29] H. Iwata, Stacking Faults in Silicon Carbide, PhD thesis, Linköping universitet (2003).
[30] M.H. Hong, A.V. Samant and P. Pirouz, Phil. Mag. A **80** 919 (2000).
[31] H. Iwata, U. Lindefelt, S. Öberg, *et al.*, Mater. Sci. Forum **389/393** 439 (2001).
[32] T.A. Kuhr, J. Liu, H.J. Chung, *et al.*, J. Appl. Phys. **92** 5863 (2002).
[33] M. Zhang, H.M. Hobgood, J.L. Demenet, *et al.*, J. Mater. Res. **18** 1087 (2003).
[34] H. Idrissi, G. Regula, M. Lancin, *et al.*, Phys. Status Solidi (c) **2** 1998 (2005).